

A context encoder for audio inpainting

Andrés Marafioti¹, Nathanaël Perraudin², Nicki Holighaus¹, and Piotr Majdak¹

¹Acoustics Research Institute, Austrian Academy of Sciences, Wohllebengasse 12–14, 1040 Vienna, Austria.

²Swiss Data Science Center, ETH Zürich, Universittstrasse 25, 8006 Zürich

Abstract

We studied the ability of deep neural networks (DNNs) to restore missing audio content based on its context, a process usually referred to as audio inpainting. We focused on gaps in the range of tens of milliseconds, a condition which has not received much attention yet. The proposed DNN structure was trained on audio signals containing music and musical instruments, separately, with 64-ms long gaps. The input to the DNN was the context, i.e., the signal surrounding the gap, transformed into time-frequency (TF) coefficients. Two networks were analyzed, a DNN with complex-valued TF coefficient output and another one producing magnitude TF coefficient output, both based on the same network architecture. We found significant differences in the inpainting results between the two DNNs. In particular, we discuss the observation that the complex-valued DNN fails to produce reliable results outside the low frequency range. Further, our results were compared to those obtained from a reference method based on linear predictive coding (LPC). For instruments, our DNNs were not able to match the performance of reference method, although the magnitude network provided good results as well. For music, however, our magnitude DNN significantly outperformed the reference method, demonstrating a generally good usability of the proposed DNN structure for inpainting complex audio signals like music. This paves the road towards future, more sophisticated audio inpainting approaches based on DNNs.

1 Introduction

Audio processing tasks often encounter locally degraded or even lost information. Some common examples are corrupted audio files, lost information in audio transmission (referred to as packet-loss in the context of Voicex-

Accompanying web page (sound examples, Matlab and Python code, color figures) www.github.com/andimarafioti/audioContextEncoder.

This work has been supported by Austrian Science Fund (FWF) project MERLIN (Modern methods for the restoration of lost information in digital signals; I 3067-N30). We gratefully acknowledge the support of NVIDIA Corporation with the donation of the Titan X Pascal GPU used for this research.

over-IP transmission), and audio signals locally contaminated by noise. Restoration of lost information in audio has been referred to as audio inpainting [1], audio interpolation [2, 3], or waveform substitution [4]. Reconstruction is usually aimed at providing a coherent and meaningful information while preventing audible artifacts so that the listener remains unaware of any occurred problem. Unfortunately, a general reconstruction of an arbitrary audio signal is nearly impossible. Thus, successful algorithms are limited to deal with a specific class of audio signals, they focus on a specific duration of the problematic signal parts, and exploit an a-priori information about the problem. In this work, we explore a new machine-learning algorithm with respect to the reconstruction of audio signals. From all possible classes of audio signals, we limit the reconstruction to instrumental music, i.e., mix of sounds from musical instruments organized in time. We focus on the duration of the problematic signal parts, i.e., *gaps*, being in the range of tens of milliseconds. Further, we exploit the available audio information surrounding the gap, i.e., the *context*.

The proposed algorithm is based on an unsupervised feature-learning algorithm driven by context-based sample prediction. It relies on a neural network with convolutional and fully-connected layers trained to generate sounds being conditioned on its context. Such an approach was first introduced for images [5] where the terminology of the *context encoder* was coined as an analogy to auto encoders [6]. Hence, we treat our algorithm as an audio-inpainting context encoder.

An application of the convolutional network directly on the time-domain audio signals requires extremely large training datasets for good results [7]. In order to reduce the size of required datasets, our context encoder works on chunks of time-frequency (TF) coefficients calculated from the time-domain audio signal. Trained with the TF coefficients, our context encoder is aimed to recover the lost TF coefficients within the gap based on provided TF coefficients of the gap’s surroundings. The TF coefficients were obtained from an invertible representation, namely, a redundant short-time Fourier transform (STFT) [8, 9], in order to allow a robust synthesis of the reconstructed

time-domain signal based on the network output.¹

Two different network structures were considered: (a) *complex network*, i.e., a network directly reconstructing the complex-valued TF coefficients which are then applied to the inverse STFT for the synthesis of the time-domain audio signal, and (b) *magnitude network*, i.e., a network reconstructing the magnitude coefficients only, which are then applied to a phase-reconstruction algorithm in order to obtain complex-valued TF coefficients required for synthesising the time-domain signal. From accurate TF magnitude information, phaseless reconstruction methods such as [10–12] are known to provide perceptually close, often indiscernable, reconstruction despite the resulting time-domain waveforms usually being rather different.

1.1 Related deep-learning techniques

Deep learning excels in classification, regression, and anomaly detection tasks [6] and has been recently successfully applied to audio [13]. Deep learning has also shown good results in generative modeling with techniques such as variational auto-encoders [14] and generative adversarial networks [15]. Unfortunately, for audio synthesis only the latter has been studied and to limited success [16]. The state-of-the-art audio signal synthesis require sophisticated networks, [17, 18] in order to obtain meaningful results. While these approaches directly predict audio samples based on the preceding samples, in the field of text-to-speech synthesizing audio in domains other than time such as spectrograms [19], and mel-spectrograms [20] have been proposed. In the field of speech transmission, DNNs have been used to achieve packet loss concealment [21].

The synthesis of *musical* audio signals using deep learning, however, is even more challenging [22]. A music signal is comprised of complex sequences ranging from short-term structures (any periodicity in the waveform) to long-term structures (like figures, motifs, or sections). In order to simplify the problem brought by long-range dependencies, music synthesis in multiple steps has been proposed including an intermediate symbolic representation like MIDI sequences [23], and features of a parametric vocoder [24].

While all of these contributions can provide insights on the design of a neural network for audio synthesis, none of them addresses the specific setting of audio inpainting where some audio information has been lost, but some of its context is known. In particular in this contribution, we explored the setting in which the the audio information surrounding a missing gap is available.

1.2 Related audio-inpainting algorithms

Audio inpainting techniques for time-domain data loss compensation can be roughly divided into two categories: (a) Methods that attempt to recover precisely the lost data relying only on very local information in the direct vicinity

¹This is in contrast to machine-learning methods solving classification tasks, in which such a synthesis is not targeted.

of the corruptions. They are usually designed for reconstructions of gap with a duration of less than 10 ms and also work well in the presence of randomly lost audio samples. (b) Methods that aim at providing a perceptually pleasing occlusion of the corruption, i.e., the corruption should not be annoying, or in the best case undetectable, for a human listener. The proposed restorations may still differ from the lost content. Such approaches are often based on self similarity, require a more global analysis of the degraded audio signal, and rely heavily on repetitive structures in audio data. They often cope with data loss beyond hundreds or even thousands of milliseconds.

In either of these categories, successful methods often depend on analyzing TF features of the audio signal instead of the time-domain signal itself. In the first category, we highlight two approaches based on the assumption that audio data is expected to possess approximately sparse time-frequency representations: In particular, variations of orthogonal matching pursuit (OMP) with time-frequency dictionaries [1, 25, 26], as well as (structured) ℓ^1 -regularization [27, 28]. They have been successfully applied to reconstruct gaps of up to 10-ms duration, however it is evident that neither of these methods is competitive when treating longer gaps. In the second class of methods, a method for packet loss concealment based on MFCC feature similarity and explicitly targeting a perceptually plausible restoration was proposed [29]. Similarly, exemplar-based inpainting was performed on a scale of seconds based on a graph encoding spectro-temporal similarities within an audio signal [30]. In both studies, gap durations where beyond several hundreds of milliseconds and their reconstruction needed to be evaluated in psychoacoustic experiments.

In our contribution, we target gap durations of tens of milliseconds, a scale where the non-stationary characteristic of audio already becomes important, but a sample-by-sample extrapolation of the missing information from the context data still seems to be realistic. The methods from category (a) can not be expected to provide good results for such long gaps, and the methods from category (b) do not aim at reconstructions on the sample-by-sample level. Interestingly, the combination of that gap durations and that level of signal reconstructions do not seem to have received much attention yet.

For simple sounds like those of musical instruments, linear prediction coding (LPC) can be applied. Assuming a modeling of the sound as an acoustic source filtered by a pole filter, extrapolation based on linear prediction has been shown to work well for gaps in the range of 5 to 100 milliseconds, e.g., [3, 31]. Although the performance of linear prediction relies heavily on the underlying stationarity assumption to be fulfilled, it seems to be the only competitive, established method in the considered scenario.

Deep-learning techniques on the other hand, some of which we study here, promise a more generalized signal representation and therefore better results, whenever the

lost data cannot be predicted by linear filtering. However, a link of deep-learning techniques with audio inpainting seems to be missing until now.

2 Context Encoder

We consider the audio signal $s \in \mathbb{R}^L$, containing L samples of audio. The central L_g samples of s represent the gap s_g , while the remaining L_c samples on each side of the gap from the context. We distinguish between s_b and s_a , which is the context signals before and after the gap, respectively.

The architecture of our network is an encoder-decoder pipeline fed with the context information. Instead of passing the time-domain signals s_b and s_a directly to the network, the audio signal is processed to obtain TF coefficients, S_b , and S_a , which is the input to the encoder. The TF representation is propagated through the encode and decoder, both trained to predict TF coefficients representing the gap, S'_g . That output of the decoder is then post-processed in order to synthesize a reconstruction in the time domain, s' .

The network structure is comprised of standard, widely-used building blocks, i.e., convolutional and fully-connected layers, and rectified linear units (ReLUs). It is inspired by the context encoder for image restoration [5].² Moreover, for the training, we do not use an adversarial discriminator, but optimize an adapted ℓ^2 -based loss.

The network was implemented in Tensorflow [33]. For the training, we applied the stochastic gradient descent solver ADAM [34]. Our software, along with instructive examples, is available to the public.³

2.1 Pre-processing stage

In the pre-processing stage, STFTs are applied on the context s_b and s_a yielding S_b and S_a , respectively. They are then split into real and imaginary parts, resulting in four channels $S_b^{Re}, S_b^{Im}, S_a^{Re}, S_a^{Im}$. The STFT is determined by the window g , hop size a and the number of frequency channels M . In our study, g was an appropriately normalized Hann window of length M and a was $M/4$, enabling perfect reconstruction by an inverse STFT with the same parameters and window. In order to obtain coefficients without artifacts even at the context borders, s_b and s_a were extended with zeros to the length of $L_c + 3a$ towards the gap.

²Before fixing the network structure described in the remainder of this section, we experimented with different architectures, depths, and kernel shapes, out of which the current structure showed the most promise. Additionally, we also considered dropout [32] and skip connections, discarding them after not achieving any notable improvements.

³www.github.com/andimarafioti/audioContextEncoder

2.2 Encoder

The encoder is a convolutional neural network. The inputs $S_b^{Re}, S_b^{Im}, S_a^{Re}, S_a^{Im}$ of the context information are treated as separate channels, thus, the network is required to learn how the channels interact and how to mix them. Similar to [5], all layers are convolutional and sequentially connected via ReLUs [35], after which batch normalization [36] is applied. The resulting encoder architecture is shown in Figure 1, for $M = 512$.

Note that because the encoder is comprised of only convolutional layers, the information can not reliably propagate from one end of the feature map to another. This is a consequence of convolutional layers connecting all the feature maps together, but never directly connecting all locations within a specific feature map [5].

2.3 Decoder

The decoder begins with a fully connected layer (FCL) with a ReLU nonlinearity in order to spread the encoder information among the channels.⁴ Similar to [5], all the subsequent layers are (de-)convolutional and, as for the encoder, connected by ReLUs with batch normalization. The network architecture is shown in Figure 2, for $M = 512$ and a gap size of 1024 samples, i.e., every output channel is of size 257×11 .

The final layer depends on the network. For the complex network, the final layer has two outputs, corresponding to the real and imaginary part of the complex-valued TF coefficients. For the magnitude network, the final layer has a single output for the magnitude TF coefficients. We denote the output TF coefficients as S'_g .

2.4 Post-processing stage

The aim of the post-processing stage is to synthesize the reconstructed audio signal in the time domain. To this end, the reconstructed gap TF coefficients from the decoder, S'_g , are inserted between the TF coefficients of the context, S_b and S_a . However, the gap between S_b and S_a is smaller than the size of S'_g because the context coefficients were calculated from zero-padded time-domain signals. The coefficients at the context border represent the zero-padded information and are discarded for synthesis, forming S'_b and S'_a . The sequence $S' = (S'_b, S'_g, S'_a)$ then has the same size as S . By performing the insertion directly in the time-frequency domain, we prevent transitional artifacts between the context and the gap, since synthesis by the inverse STFT introduces an inherent cross-fading.

For the complex network, the decoder output represents the real and imaginary parts of complex-valued TF coef-

⁴Fully connected layers are computationally very expensive; in our case it contains 38% of all the parameters of the network. In [5], this issue was addressed by using a 'channel-wise fully connected layer'. We tested that approach but obtained consistently worse results.

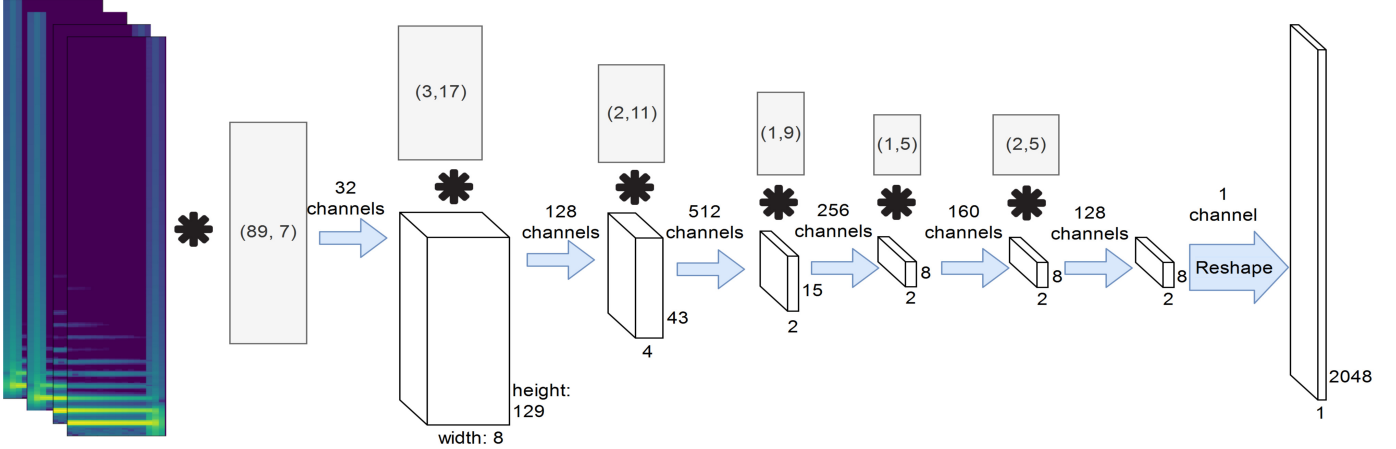


Figure 1: The encoder is a convolutional network with six layers followed by reshaping. The four channel time-frequency input is transformed into an encoding of size 2048. Gray rectangles represent the convolution filters with size expressed as (height, width). White cubes represent the signal.

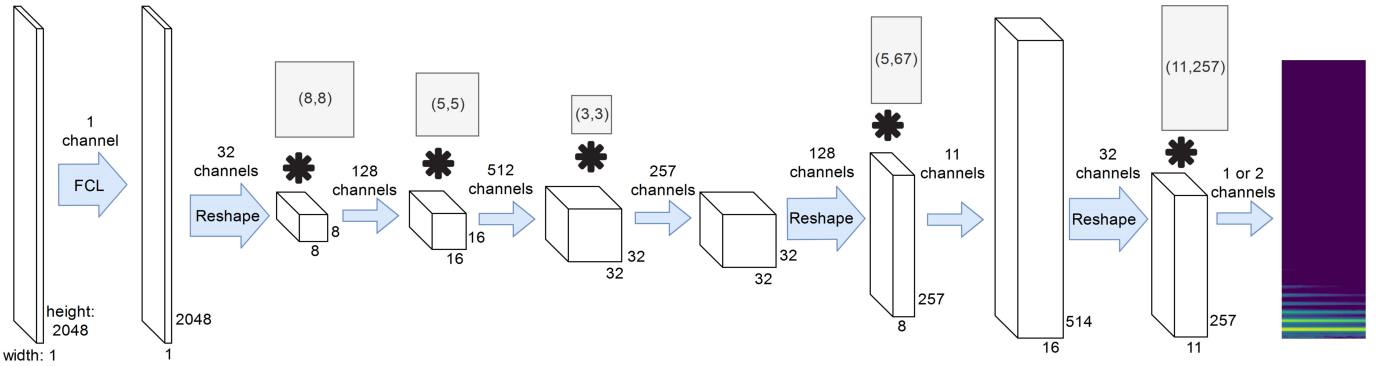


Figure 2: The decoder generates (complex or magnitude) time-frequency coefficients from the encoding produced by the encoder, Fig. 1. It consists of a fully connected layer (FCL) and five deconvolution layers, with reshaping after the fully-connected, as well as the third and fourth deconvolution layers. All other conventions as in Figure 1.

ficients S'_g and the inverse STFT can be directly applied yielding s' .

For the magnitude network, the decoder output represents the magnitudes of the TF coefficients and the missing phase information needs to be estimated separately. First, the phase gradient heap integration algorithm proposed in [37] was applied to the magnitude coefficients produced by the decoder in order to obtain an initial estimation of the TF phase. Then, this estimation was refined by applying 100 iterations of the fast Griffin-Lim algorithm [10, 11] implemented in the Phase Retrieval Toolbox Library [38].⁵ The resulting complex-valued TF coefficients S'_g were then transformed into a time-domain signal s' by inverse STFT.

2.5 Loss Function

The network training is based on the minimization of the total loss of the reconstruction. Generally, we computed the reconstruction loss by comparing the original gap TF coefficients S_g with the reconstructed gap TF coefficients S'_g . The comparison is then done on the basis of the squared ℓ^2 -norm of the difference between S_g and S'_g as it is customary for this type of network [39], commonly known as mean squared error (MSE). The absolute MSE depends, however, on the total energy of S_g , clearly putting more weight on signals containing more energy.

In contrast, the comparison can be done by using the normalized mean squared error (NMSE),

$$\text{NMSE}(S_g, S'_g) = \frac{\|S_g - S'_g\|^2}{\|S_g\|^2} \quad (1)$$

⁵The combination of these two algorithms provided consistently better results than separate application of either.

While theoretically invariant to amplitude changes, this measure strongly amplifies small errors when the energy of

S_g is small. In practice, however, very minor deviations from S_g are insignificant regardless of the content of S_g , which is not reflected in NMSE.

Therefore, we propose to use a weighted mix between MSE and NMSE for the calculation of the loss function. This leads to

$$\mathbf{F}(S_g, S'_g) = \frac{\|S_g - S'_g\|^2}{c^{-1} + \|S_g\|^2}, \quad (2)$$

where the constant $c > 0$ controls the incorporated compensation for small amplitude. In our experiments, $c = 5$ yielded good results.

Finally, as proposed in [40], the total loss is the sum of the loss function and a regularization term controlling the trainable weights in terms of their ℓ^2 -norm:

$$\mathbf{T} = F(S_g, S'_g) + \frac{\lambda}{2} \sum_i w_i^2, \quad (3)$$

with w_i being weights of the network and λ being the regularization parameter, here set to 0.01.

3 Evaluation

The main objectives of the evaluation were to investigate the general ability of the networks to adapt to the considered class of audio signals, as well as how they compare to the reference method, i.e., LPC-based extrapolation as proposed in [31]. Additionally, we considered the effects of changing the gap duration and the networks' ability to generate pure sine tones.

To this end, we considered three classes of audio signals: pure tones, instrument sounds, and music. For instruments and music, the respective networks were trained on the targeted signal class, with an assumed gap size of 64 ms. Reconstruction was evaluated on the trained signal class and pure tones for 64 ms gaps. Additionally, the magnitude network was evaluated for 48 ms gaps. Reconstruction quality was evaluated by means of signal-to-noise ratios (SNR) applied to the time-domain waveforms and magnitude spectrograms, where the latter is introduced to accommodate for perceptually irrelevant phase changes. Further, all results were compared to the reconstruction based on the reference method.

3.1 Parameters

The sampling rate was 16 kHz. We considered audio segments with a duration of 320 ms, which corresponds to $L = 5120$ samples. Each segment was separated in a gap of 64 ms (or 48 ms, corresponding to $L_g = 1024$ or $L_g = 768$ samples) of the central part of a segment and the context of twice of 128 ms (or 136 ms), corresponding to $L_c = 2048$ (or $L_c = 2176$) samples. Both, the size of the window g and the number of frequency channels M were fixed to 512 samples. Consequently, a was 128 samples, and the input to the encoder was $S_b, S_a \in \mathbb{C}^{257 \times 16}$.

3.2 Datasets

The pure tones were directly synthesized as sine oscillations. We used a logarithmic frequency range from 20 Hz to 8 kHz, linear phase shift range from 0 to π , and linear amplitude range from 0.1 to 1. The duration was 320 ms corresponding to 5120 samples at the sampling rate of 16 kHz. Because of their simplicity, we do not treat pure tones as a training dataset, but rather use them to evaluate the behavior of the system.

The dataset representing musical instruments was derived from the NSynth dataset [41]. NSynth is an audio dataset containing 305,979 musical notes from 1,006 instruments, each with a unique pitch, timbre, and envelope. Each example is four seconds long, monophonic, and sampled at 16 kHz.

The dataset representing music was derived from the free music archive (FMA) [42]. The FMA is an open and easily accessible dataset, usually used for evaluating tasks in musical information retrieval (MIR). We used the small version of the FMA comprised of 8,000 30-s segments of songs with eight balanced genres sampled at 44.1 kHz. We resampled each segment to the sampling rate of 16 kHz.

The original segments in the two datasets were processed to fit the evaluation parameters. First, for each example the silence was removed. Second, from each example, pieces of the duration of 320 ms were copied, starting with the first segment at the beginning of a segment, continuing with further segments with a shift of 32 ms. Thus, each example yielded multiple overlapping segments s . Note that for a gap of 64 ms, the segment can be considered as a 3-tuple by labeling the first 128 ms as the context before the gap s_b , the subsequent 64 ms as the gap s_g , and the last 128 ms as the context after the gap s_a . Finally, all segments with RMS smaller than ten to the negative four in s_g were discarded.

The datasets were split into training, validation, and testing sets. For the instruments, we used the splitting proposed by [41]. The music dataset, was split into approximately 70%, 20% and 10%, respectively. The statistics of the resulting sets are presented in Table 1.

| | Count | Percentage |
|------------------------|-------|------------|
| Instruments training | 19.4M | 94.1 |
| Instruments validation | 0.9M | 4.4 |
| Instruments testing | 0.3M | 1.5 |
| Music training | 5.2M | 70.0 |
| Music validation | 1.5M | 20.0 |
| Music testing | 0.7M | 10.0 |

Table 1: Datasets used in the evaluation.

3.3 Training

Both complex and magnitude networks were trained, each of them separately for the instrument and music dataset. This resulted in four trained networks.

Each training started with the learning rate of 10^{-3} . In the case of the magnitude network, the reconstructed phase was not considered in the training. Every 2000 steps, the training progress was monitored. To this end, the network's output was calculated for the music validation dataset and the NMSE was calculated between the predicted and the actual TF coefficients of the gap. When converging, which usually happened after approximately 600k steps, the learning rate was reduced to 10^{-4} and the training was continued by additional 200k steps.⁶

3.4 Evaluation metrics

For the evaluation of our results, in general, we calculated the SNR (in dB)

$$\text{SNR}(x, x') = 10 \log \frac{\|x\|^2}{\|x - x'\|^2} \quad (4)$$

for each segment of a testing dataset separately, and then averaged all these SNR across all segments of that testing dataset.

For the evaluation in the time domain, we used $\text{SNR}(s_g, s'_g)$, which is the SNR calculated on the gaps of the actual and reconstructed signals, s_g and s'_g , respectively. We refer to the average of this metric across all segments to as SNR in the time domain (SNR_{TD}).

For the evaluation in the TF domain, we calculated $\text{SNR}(|S_g|, |S_{rg}|)$, where S_{rg} represents the central 5 frames of the STFT computed from the restored signal s' and thus represents the restoration of the gap. In other words, we compute the SNR between the spectrograms of the original signal and the restored signal, but only in the region of the gap. We refer to the average of this metric (across all segments of a testing dataset) to as SNR_{MS} , where MS references to magnitude spectrogram. Note that SNR_{MS} is directly related to the logarithmic inverse of the spectral convergence proposed in [43].

3.5 Reference method

We compared our results to those obtained with a reference method based on LPC [44]. LPC is particularly widely used for the processing of speech [45], but also frequently for extrapolation of audio signals [2, 31].

For the implementation, we followed [31], especially [31, Section 5.3]. In detail, the context signals s_b and s_a were extrapolated onto the gap s_g by computing their impulse responses and using them as prediction filters for a classical linear predictor. The impulse responses were obtained using Burg's Method [46] and were fixed to have 1000 coefficients according to the suggestions from [2] and [47].

⁶We also considered training on the instrument training dataset (800k steps) followed by a refinement with the music training dataset (300k steps). While it did not show substantial differences to the training performed on music only, a pre-trained network on instruments with a subsequent refinement to music may be an option in applications addressing a specific music genre.

Their duration was the same as that for our context encoder in order to provide the same amount of context information. The two extrapolations were mixed with the squared-cosine weighting function. Our implementation of the LPC extrapolation is available online⁷.

Finally, we evaluate the results produced by the reference method in the same way as we evaluate the results produced by the networks: predictions were calculated for each segment from both testing datasets and the SNR_{TD} as well as the SNR_{MS} were calculated on the predictions.

4 Results and discussion

4.1 Ability to adapt to the training material

A network able to adapt to the trained material will perform better on the trained material than on signals new to the network. Our network was trained on instruments mostly consisting of discrete frequencies arranged in time. If our network was able to adapt to the instruments then it should perform on these frequencies better than on others. To this end, we probed our trained networks with pure tones of various frequencies.

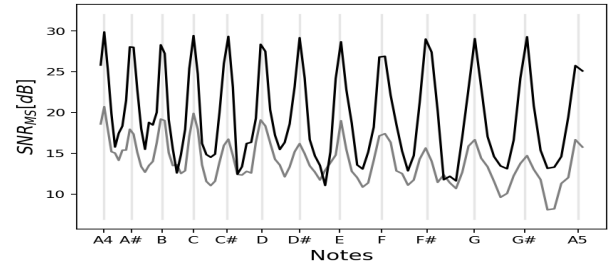


Figure 3: SNR_{MS} for reconstruction of pure tones with the complex network trained on the instrument (black) and music (grey) dataset. SNR are shown as a function of musical notes corresponding to the Standard pitch, i.e., the note A4 corresponds to the frequency of 440 Hz.

Figure 3 shows the SNR_{MS} of the reconstruction obtained with the complex network. The abscissa shows notes, i.e., frequencies corresponding to the Standard pitch (with A corresponding to the frequency of 440 Hz). For the network trained on the instruments, the SNR_{MS} was large in the proximity of notes and decreased by more than 15 dB for frequencies between the notes. This shows that the network was able to better predict signals corresponding to the trained notes, indicating a good adaptation to the trained material.

Music contains broadband sounds like drums, breathing, tone glides, etc, i.e., sounds with nonsignificant energy at frequencies between the Standard pitch. A network trained

⁷www.github.com/andimarafioti/audioContextEncoder

to music is expected to be less sensitive to predictions performed on standard pitch only. Figure 3 shows thus also the SNR_{MS} obtained for the reconstruction of pure tone with the network trained on the music. The SNR_{MS} fluctuations were smaller than those from the network trained on the instruments. This further supports our conclusion about the good ability of our network structure to adapt to various training materials.

4.2 Effect of the network type

The difference between the magnitude and complex networks both trained on instruments can be anticipated from the Figure 4, which shows the SNR_{MS} of the reconstructions of pure tones. As an average over frequency, the magnitude network provided an SNR_{MS} of 10.2 dB larger than that of the complex network. For the magnitude network, the SNR_{MS} was more or less similar for frequencies up to 200 Hz and decreased with frequency. For the complex network, the SNR_{MS} decrease started already at approximately 100 Hz and was much steeper than that of the magnitude network. Above the frequency of approximately 4 kHz, the complex network provided an extremely poor SNR_{MS} of 5 dB or less, indicating that the complex network had problems reconstructing the signals at higher frequencies. This is in line with [48], where neural networks were trained to reconstruct phases of amplitude spectrograms and their predictions were also poorer for higher frequencies.

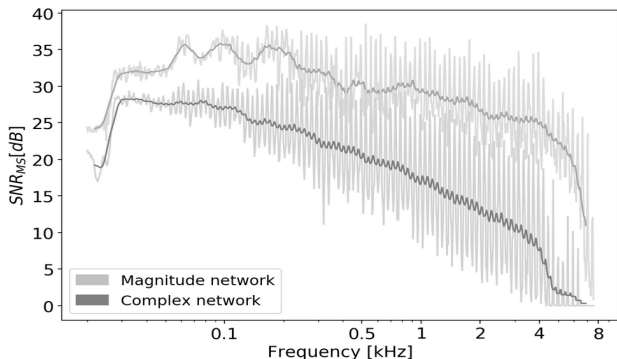


Figure 4: SNR_{MS} for reconstruction of pure tones with the complex (black) and magnitude (grey) networks both trained to the instruments database. The thicker lines show averages over 25 surrounding frequency points.

Unfortunately, the problem of poor high-frequency reconstruction also persisted when predicting instrument sounds instead of pure tones. Figure 5 shows the spectrogram of an original sound from the instrument testing set (left panel) and of its reconstruction obtained from the complex network (center panel). The reconstruction clearly fails at frequencies higher than 4 kHz.

In order to further compare between the two network types, reconstructions of the testing datasets were per-

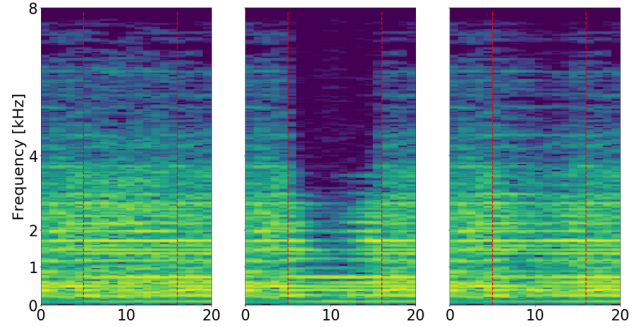


Figure 5: Magnitude spectrograms (in dB) of an exemplary signal reconstruction. Left: Original signal. Center: Reconstruction by the complex network. Right: Reconstruction by the LPC-based method. The gap was the area between the two red lines.

formed. Table 2 shows the SNR_{MS} of those predictions. The magnitude network resulted in consistently better results with a difference of 2.5 dB and 3.5 dB when tested on music and instruments, respectively. This might be associated with the complex network having problems at high frequencies. Although it might seem that this comparison is flawed, because the magnitude network has access to almost the same number of neurons to predict only half as many features, it cannot be expected that doubling the size of the complex network yields significantly better predictions, as the link between the size of a DNN and its performance is not proportional [49].

In addition to the improvement in SNR_{MS} of the magnitude network over the complex network, the complex network predictions were observed to often be corrupted by clearly audible broadband noise⁸, which was not found in the solutions of the magnitude network.

| | Music | | | Instruments | | |
|------|-------|------|-----|-------------|------|------|
| | Mag | Comp | LPC | Mag | Comp | LPC |
| Mean | 7.7 | 5.2 | 6.3 | 22.0 | 18.5 | 30.6 |
| Std | 4.3 | 4.4 | 5.1 | 10.4 | 10.2 | 18.9 |

Table 2: SNR_{MS} (in dB) of reconstructions of 64 ms gaps for the complex and magnitude networks, as well as for the LPC-based method.

4.3 Comparison to the reference method

Table 2 provides the SNR_{MS} for the LPC-based reference reconstruction method. When tested on music, on average, the magnitude network outperformed the LPC-based method by 1.4 dB. When tested on instruments, the magnitude network underperformed by 8.6 dB.

⁸For audio examples, please visit: www.github.com/andimarfioti/audioContextEncoder

When looking more in the details of the reconstruction, both methods showed different characteristics: In Figure 6 we show spectrograms of an instrument signal with frequency-modulated components. The LPC-based reconstruction shows a discontinuity in the middle of the gap instead of a steady transition. This is the consequence of the two extrapolations (forward and backwards), mixed in the middle of the gap. The magnitude network trained on the music learned how to represent frequency modulations and provides less artifacts in the reconstruction, which yielded a 5 dB larger SNR_{MS} .

Another interesting examples are shown in Figure 7. The top row shows an example in which the magnitude network outperformed the LPC-based method. In this case, the signal is comprised of steady harmonic tones in the left side context and a broadband sound in the right side context. While the LPC-based method extrapolated the broadband noise into the gap, the magnitude network was able to foresee the transition from the steady sounds to the broadband burst, yielding a prediction much closer to the original gap, with a 13 dB larger SNR_{MS} than that from the LPC-based method.

On the other hand, the magnitude network not always outperformed the LPC-based method. The bottom row of Figure 7 shows spectrograms of such an example. This signal had stable sounds in the gap, which were well-suited for an extrapolation, but rather complex to be perfectly reconstructed by the magnitude network. Thus, the LPC-based method outperformed the magnitude network yielding a 9 dB larger SNR_{MS} .

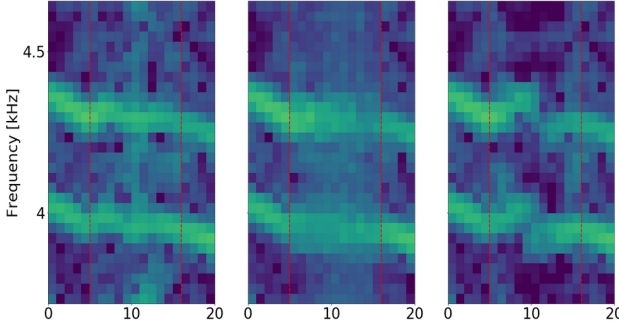


Figure 6: Sections of magnitude spectrograms (in dB) of an exemplary signal reconstruction. Left: Original signal. Center: Reconstruction by the magnitude network. Right: Reconstruction by the LPC-based method. The magnitude network provided a 5 dB larger SNR_{MS} .

Finally, Table 3 presents the SNR_{TD} of reconstructions of the instrument and music. Note that the SNR_{TD} provided for the magnitude network is for the sake of completeness only. The SNR_{TD} metric is highly sensitive to phase differences, which do not necessarily lead to perceptual differences and, for the magnitude network, is reconstructed with an accuracy of up to a constant phase shift. Thus, SNR_{TD} can remain low even in cases of very good

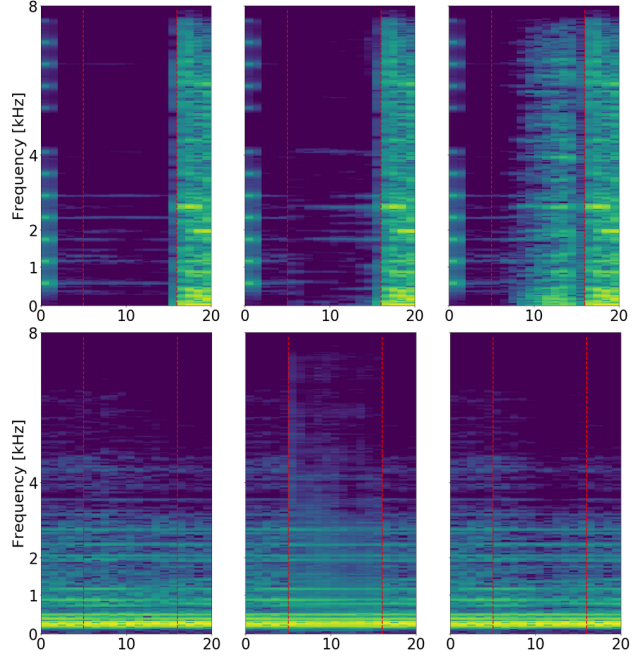


Figure 7: Magnitude spectrograms (in dB) of exemplary signal reconstructions. Left: Original signal. Center: Reconstruction by the magnitude network. Right: Reconstruction by the LPC-based method. Top: Example with the magnitude network outperforming the reference by an SNR_{MS} of 13 dB. Bottom: Example with the magnitude network underperforming the reference by an SNR_{MS} of 9 dB.

reconstructions. Hence, here, we compare the performance of the complex network with that of the LPC-based method only.

For the music, on average, the complex network outperformed the LPC-based method providing a 0.3 dB larger SNR_{TD} . Given the large standard deviation, we performed a pair t-test on the SNR_{TD} which showed that the difference was statistically significant ($p < 0.001$). For the instruments, on average, the LPC-based reconstruction outperformed our network by 12 dB.

The excellent performance of the LPC-based method reconstructing instruments can be explained by the assumptions behind the LPC well-fitting to the single-note instrument sounds. These sounds usually consist of harmonics stable on a short-time scale. LPC extrapolates these harmonics preserving the spectral envelope of the signal. Nevertheless, the magnitude network yielded an SNR_{MS} of 22.0 dB, on average, demonstrating a good ability to reconstruct instrument sounds.

When applied on music, the performance of both methods was much poorer, with our network performing slightly but statistically significantly better than the LPC-based method. The better performance of our network can be explained by its ability to adapt to transient sounds and modulations in frequencies, sound properties that the LPC-

based method is not suited to handle.

| | Music | | | Instruments | | |
|------|-------|-----|-----|-------------|------|------|
| | Comp | Mag | LPC | Comp | Mag | LPC |
| Mean | 3.8 | 0.6 | 3.5 | 16.0 | 13.0 | 28.0 |
| Std | 4.1 | 3.7 | 5.0 | 9.7 | 10.3 | 19.1 |

Table 3: SNR_{TD} (in dB) of reconstructions of 64 ms gaps for the complex and magnitude networks, as well as for the LPC-based method.

4.4 Effect of the gap duration

The proposed network structure can be trained with different contexts and gap durations. For problems of varying gap duration, a network trained to the particular gap duration might appear optimal. However, training takes time, and it might be simpler to train a network to single gap duration and use it to reconstruct any shorter gap as well.

In order to test this idea, we introduced gaps of 48 ms in our testing datasets. These gaps were then reconstructed by the magnitude network trained for 64 ms gaps. As this network outputs, at reconstruction time, a solution for a gap of length 64-ms, the 48-ms gaps needs to be extended. We tested three types of the extension: 16 ms forwards, 16 ms backwards, and centered (8 ms forwards and 8 ms backwards).

Table 4 shows SNR_{MS} obtained from reconstructions of the three types of gap extension, as averages over these extension types. Also, the corresponding SNR_{MS} for the LPC-based method are shown. The results are similar to those obtained for larger gaps: for the instruments, the LPC-based method outperformed our network; for the music, our network outperformed the LPC-based method.

| | Music | | Instruments | |
|------|-------|-----|-------------|------|
| | Ours | LPC | Ours | LPC |
| Mean | 8.0 | 6.9 | 21.6 | 33.2 |
| Std | 4.6 | 5.5 | 11.5 | 20.1 |

Table 4: SNR_{MS} (in dB) of reconstructions of 48 ms gaps for the magnitude network and the LPC-based method.

5 Conclusions and Outlook

We proposed a convolutional neural network architecture working as a context encoder on TF coefficients. For the reconstruction of complex signals like music, that network was able to outperform the LPC-based reference method, in terms SNR calculated on magnitude spectrograms. However, LPC yielded better results when applied on more simple signals like instrument sounds. We have further shown that the proposed network was able to adapt to the particular pitches provided by the training material

and that it can be applied to gaps shorter than the trained ones. In general, our results suggest that standard components and a moderately sized network can be applied to form audio-inpainting models, offering a number of angles for future improvement.

For example, we have analyzed two types of networks. The complex network works directly on the complex-valued TF coefficients. The magnitude network provides only magnitudes of TF coefficients as output and relies on a subsequent phase reconstruction. We observed clear improvement of the magnitude network over the complex network especially in reconstructing high-frequency content.

Training a generative method directly on audio data requires vast size of datasets and large networks. To construct more compact models of moderately sized datasets, it is imperative to use efficient input audio features and an invertible feature representation at the output. Here, the STFT features, meant as a reasonable first choice, provided a decent performance. In the future, we expect more hearing-related features to provide even better reconstructions. In particular, an investigation of Audlet frames, i.e., invertible time-frequency systems adapted to perceptual frequency scales, [50], as features for audio inpainting present intriguing opportunities.

Generally, better results can be expected for increased depth of the network and the available context. Unfortunately, our preliminary tests of simply increasing the network’s depth led to minor improvements only. As it seems, a careful consideration of the building blocks of the model is required instead. Here, preferred architectures are those not relying on a predetermined target and input feature length, e.g., a recurrent network. Recent advances in generative networks will provide other interesting alternatives for analyzing and processing audio data as well. These approaches are yet to be fully explored.

Finally, music data can be highly complex and it is unreasonable to expect a single trained model to accurately inpaint a large number of musical styles and instruments at once. Thus, instead of training on a very general dataset, we expect significantly improved performance for more specialized networks that could be trained by restricting the training data to specific genres or instrumentation. Applied to a complex mixture and potentially preceded by a source-separation algorithm, the resulting models could be used jointly in a mixture-of-experts, [51], approach.

References

- [1] A. Adler, V. Emiya, M. G. Jafari, M. Elad, R. Gribonval, and M. D. Plumley, “Audio inpainting,” *IEEE Transactions on Audio, Speech, and Language Processing*, vol. 20, no. 3, pp. 922–932, March 2012.
- [2] I. Kauppinen, J. Kauppinen, and P. Saarinen, “A method for long extrapolation of audio signals,” *Jour-*

nal of the Audio Engineering Society, vol. 49, no. 12, pp. 1167–1180, 2001.

[3] W. Etter, “Restoration of a discrete-time signal segment by interpolation based on the left-sided and right-sided autoregressive parameters,” *IEEE Transactions on Signal Processing*, vol. 44, no. 5, pp. 1124–1135, may 1996.

[4] D. Goodman, G. Lockhart, O. Wasem, and W.-C. Wong, “Waveform substitution techniques for recovering missing speech segments in packet voice communications,” *IEEE Transactions on Acoustics, Speech, and Signal Processing*, vol. 34, no. 6, pp. 1440–1448, dec 1986.

[5] D. Pathak, P. Krahenbuhl, J. Donahue, T. Darrell, and A. Efros, “Context encoders: Feature learning by inpainting.”

[6] I. Goodfellow, Y. Bengio, and A. Courville, *Deep Learning*. MIT Press, 2016, <http://www.deeplearningbook.org>.

[7] J. Pons, O. Nieto, M. Prockup, E. M. Schmidt, A. F. Ehmann, and X. Serra, “End-to-end learning for music audio tagging at scale,” *CoRR*, vol. abs/1711.02520, 2017. [Online]. Available: <http://arxiv.org/abs/1711.02520>

[8] M. Portnoff, “Implementation of the digital phase vocoder using the fast fourier transform,” *IEEE Trans. Acoust. Speech Signal Process.*, vol. 24, no. 3, pp. 243–248, 1976.

[9] K. Gröchenig, *Foundations of Time-Frequency Analysis*, ser. Appl. Numer. Harmon. Anal. Birkhäuser, 2001.

[10] D. Griffin and J. Lim, “Signal estimation from modified short-time fourier transform,” *IEEE Transactions on Acoustics, Speech, and Signal Processing*, vol. 32, no. 2, pp. 236–243, 1984.

[11] N. Perraudeau, P. Balazs, and P. L. Søndergaard, “A fast griffin-lim algorithm,” in *Applications of Signal Processing to Audio and Acoustics (WASPAA), 2013 IEEE Workshop on*. IEEE, 2013, pp. 1–4.

[12] Z. Průša, P. Balazs, and P. Søndergaard, “A noniterative method for reconstruction of phase from stft magnitude,” *IEEE/ACM Transactions on Audio, Speech, and Language Processing*, vol. 25, no. 5, pp. 1154–1164, 2017.

[13] J. Schlueter, “Deep Learning for Event Detection, Sequence Labelling and Similarity Estimation in Music Signals,” Ph.D. dissertation, Johannes Kepler University Linz, Austria, Jul. 2017.

[14] D. Kingma and M. Welling, “Auto-encoding variational bayes.” *CoRR*, vol. abs/1312.6114, 2013.

[15] I. Goodfellow, J. Pouget-Abadie, M. Mirza, B. Xu, D. Warde-Farley, S. Ozair, A. Courville, and Y. Bengio, “Generative adversarial nets,” in *Advances in neural information processing systems*, 2014, pp. 2672–2680.

[16] C. Donahue, J. McAuley, and M. Puckette, “Synthesizing Audio with Generative Adversarial Networks,” *ArXiv e-prints*, Feb. 2018.

[17] S. Mehri, K. Kumar, I. Gulrajani, R. Kumar, S. Jain, J. Sotelo, A. Courville, and Y. Bengio, “Samplernn: An unconditional end-to-end neural audio generation model,” *CoRR*, vol. abs/1612.07837, 2016. [Online]. Available: <http://arxiv.org/abs/1612.07837>

[18] A. van den Oord, S. Dieleman, H. Zen, K. Simonyan, O. Vinyals, A. Graves, N. Kalchbrenner, A. Senior, and K. Kavukcuoglu, “Wavenet: A generative model for raw audio,” *CoRR*, vol. abs/1609.03499, 2016. [Online]. Available: <http://arxiv.org/abs/1609.03499>

[19] Y. Wang, R. Skerry-Ryan, D. Stanton, Y. Wu, R. Weiss, N. Jaitly, Z. Yang, Y. Xiao, Z. Chen, S. Bengio, Q. Le, Y. Agiomyrgiannakis, R. Clark, and R. Saurous, “Tacotron: A fully end-to-end text-to-speech synthesis model,” *CoRR*, vol. abs/1703.10135, 2017.

[20] J. Shen, R. Pang, R. Weiss, M. Schuster, N. Jaitly, Z. Yang, Z. Chen, Y. Zhang, Y. Wang, R. Skerry-Ryan, R. Saurous, Y. Agiomyrgiannakis, and Y. Wu, “Natural TTS synthesis by conditioning wavenet on mel spectrogram predictions,” *CoRR*, vol. abs/1712.05884, 2017. [Online]. Available: <http://arxiv.org/abs/1712.05884>

[21] B.-K. Lee and J.-H. Chang, “Packet loss concealment based on deep neural networks for digital speech transmission,” *IEEE/ACM Trans. Audio, Speech and Lang. Proc.*, vol. 24, no. 2, pp. 378–387, Feb. 2016. [Online]. Available: <http://dx.doi.org/10.1109/TASLP.2015.2509780>

[22] S. Dieleman, A. v. d. Oord, and K. Simonyan, “The challenge of realistic music generation: modelling raw audio at scale,” *arXiv preprint arXiv:1806.10474*, 2018.

[23] N. Boulanger-Lewandowski, Y. Bengio, and P. Vincent, “Modeling temporal dependencies in high-dimensional sequences: Application to polyphonic music generation and transcription,” in *ICML*, 2012.

[24] M. Blaauw and J. Bonada, “A neural parametric singing synthesizer,” *CoRR*, vol. abs/1704.03809, 2017. [Online]. Available: <http://arxiv.org/abs/1704.03809>

[25] A. Adler, V. Emiya, M. Jafari, M. Elad, R. Gribonval, and M. Plumley, “A constrained matching pursuit approach to audio declipping,” in *IEEE International Conference on Acoustics, Speech and Signal Processing (ICASSP)*, may 2011.

[26] I. Toumi and V. Emiya, “Sparse non-local similarity modeling for audio inpainting,” in *ICASSP - IEEE International Conference on Acoustics, Speech and Signal Processing*, Calgary, Canada, Apr. 2018.

[27] K. Siedenburg, M. Dörfler, and M. Kowalski, “Audio inpainting with social sparsity,” *SPARS (Signal Processing with Adaptive Sparse Structured Representations)*, 2013.

[28] F. Lieb and H.-G. Stark, “Audio inpainting: Evaluation of time-frequency representations and structured sparsity approaches,” *Signal Processing*, vol. 153, pp. 291–299, 2018.

[29] Y. Bahat, Y. Schechner, and M. Elad, “Self-content-based audio inpainting,” *Signal Processing*, vol. 111, pp. 61–72, jun 2015.

[30] N. Perraudin, N. Holighaus, P. Majdak, and P. Balazs, “Inpainting of long audio segments with similarity graphs,” *IEEE/ACM Transactions on Audio, Speech, and Language Processing*, vol. PP, no. 99, pp. 1–1, 2018.

[31] I. Kauppinen and K. Roth, “Audio signal extrapolation—theory and applications,” in *Proc. DAFx*, 2002, pp. 105–110.

[32] N. Srivastava, G. Hinton, A. Krizhevsky, I. Sutskever, and R. Salakhutdinov, “Dropout: a simple way to prevent neural networks from overfitting,” *The Journal of Machine Learning Research*, vol. 15, no. 1, pp. 1929–1958, 2014.

[33] M. Abadi, A. Agarwal, P. Barham, E. Brevdo, Z. Chen, C. Citro, G. Corrado, A. Davis, J. Dean, M. Devin, S. Ghemawat, I. Goodfellow, A. Harp, G. Irving, M. Isard, Y. Jia, R. Jozefowicz, L. Kaiser, M. Kudlur, J. Levenberg, D. Mané, R. Monga, S. Moore, D. Murray, C. Olah, M. Schuster, J. Shlens, B. Steiner, I. Sutskever, K. Talwar, P. Tucker, V. Vanhoucke, V. Vasudevan, F. Viégas, O. Vinyals, P. Warden, M. Wattenberg, M. Wicke, Y. Yu, and X. Zheng, “TensorFlow: Large-scale machine learning on heterogeneous systems,” 2015, software available from tensorflow.org. [Online]. Available: <https://www.tensorflow.org/>

[34] D. Kingma and J. Ba, “Adam: A method for stochastic optimization.”

[35] P. Ramachandran, B. Zoph, and Q. Le, “Searching for activation functions.”

[36] S. Ioffe and C. Szegedy, “Batch normalization: Accelerating deep network training by reducing internal covariate shift,” *CoRR*, vol. abs/1502.03167, 2015.

[37] Z. Průša and P. L. Søndergaard, “Real-Time Spectrogram Inversion Using Phase Gradient Heap Integration,” in *Proc. Int. Conf. Digital Audio Effects (DAFx-16)*, Sep 2016, pp. 17–21.

[38] Z. Průša, “The Phase Retrieval Toolbox,” in *AES International Conference On Semantic Audio*, Erlangen, Germany, June 2017.

[39] H. Zhao, O. Gallo, I. Frosio, and J. Kautz, “Loss functions for image restoration with neural networks,” *IEEE Transactions on Computational Imaging*, vol. 3, no. 1, pp. 47–57, March 2017.

[40] A. Krogh and J. Hertz, “A simple weight decay can improve generalization,” in *Advances in neural information processing systems 4*. Morgan Kaufmann, 1992, pp. 950–957.

[41] J. Engel, C. Resnick, A. Roberts, S. Dieleman, D. Eck, K. Simonyan, and M. Norouzi, “Neural audio synthesis of musical notes with wavenet autoencoders,” 2017.

[42] M. Defferrard, K. Benzi, P. Vandergheynst, and X. Bresson, “Fma: A dataset for music analysis,” in *18th International Society for Music Information Retrieval Conference*, 2017.

[43] N. Sturmel and L. Daudet, “Signal reconstruction from stft magnitude: A state of the art,” in *International conference on digital audio effects (DAFx)*, 2011, pp. 375–386.

[44] T. E. Tremain, “The government standard linear predictive coding algorithm: Lpc-10,” *Speech Technology*, pp. 40–49, Apr. 1982.

[45] M. Rajman and V. Pallotta, *Speech and language engineering*. EPFL Press, 2007.

[46] J. P. Burg, “Maximum entropy spectral analysis,” *37th Annual International Meeting, Soc. of Explor. Geophys., Oklahoma City*, 1967.

[47] I. Kauppinen and J. Kauppinen, “Reconstruction method for missing or damaged long portions in audio signal,” *Journal of the Audio Engineering Society*, vol. 50, no. 7/8, pp. 594–602, 2002.

[48] S. Takamichi, Y. Saito, N. Takamune, D. Kitamura, and H. Saruwatari, “Phase reconstruction from amplitude spectrograms based on von-mises-distribution deep neural network,” *arXiv preprint arXiv:1807.03474*, 2018.

- [49] K. He, X. Zhang, S. Ren, and J. Sun, “Deep residual learning for image recognition,” in *2016 IEEE Conference on Computer Vision and Pattern Recognition (CVPR)*, June 2016, pp. 770–778.
- [50] T. Necciari, N. Holighaus, P. Balazs, Z. Pra, P. Majdak, and O. Derrien, “Audlet filter banks: A versatile analysis/synthesis framework using auditory frequency scales,” *Applied Sciences*, vol. 8, no. 1:96, 2018.
- [51] S. E. Yuksel, J. N. Wilson, and P. D. Gader, “Twenty years of mixture of experts,” *IEEE transactions on neural networks and learning systems*, vol. 23, no. 8, pp. 1177–1193, 2012.